International Journal of Extreme Manufacturing

Pulsed current-assisted twelve-roll precision rolling deformation of SUS304 ultra-thin strips with exceptional mechanical properties

To cite this article before publication: wanwan Fan *et al* 2024 *Int. J. Extrem. Manuf.* in press https://doi.org/10.1088/2631-7990/ad4073

Pulsed current-assisted twelve-roll precision rolling deformation of SUS304 ultra-thin strips with exceptional mechanical properties

Journal:	*International Journal of Extreme Manufacturing*
Manuscript ID	IJEM-111410.R1
Manuscript Type:	Paper
Keywords:	pulsed current-assisted, SUS304 ultra-thin strip, rolling reduction rate, work-hardening, mechanical properties

Pulsed current-assisted twelve-roll precision rolling deformation of SUS304 ultra-thin strips with exceptional mechanical properties

Wanwan Fan[1,2], Tao Wang[1,2,3,*], Jinxiong Hou[1,2,3], Zhongkai Ren[1,2,3], Qingxue Huang[1,2,3] and Guanghui Wu[4]

[1] College of Mechanical and Vehicle Engineering, Taiyuan University of Technology, Yingze West Street 79, Taiyuan, 030024, Shanxi Province, People's Republic of China

[2] Engineering Research Center of Advanced Metal Composites Forming Technology and Equipment of Ministry of Education, Taiyuan University of Technology, Yingze West Street 79, Taiyuan, 030024, Shanxi Province, People's Republic of China

[3] National Key Laboratory of Metal Forming Technology and Heavy Equipment, Taiyuan University of Technology, Yingze West Street 79, Taiyuan, 030024, Shanxi Province, People's Republic of China

[4] College of Aeronautics and Astronautics, Taiyuan University of Technology, Yingze West Street 79, Taiyuan, 030024, Shanxi Province, People's Republic of China

E-mail: **twang@tyut.edu.cn**

Abstract

Innovative pulsed current-assisted multi-pass rolling tests were conducted on a twelve-roll mill during the rolling deformation processing of SUS304 ultra-thin strips. The results show that in the first rolling pass, the rolling reduction rate of a conventionally rolled sample (at room temperature) is 33.8%, which can be increased to 41.5% by pulsed current-assisted rolling, enabling the formation of an ultra-thin strip with a size of 67.3 μm in only one rolling pass. After three passes of pulsed current-assisted rolling, the thickness of the ultra-thin strip can be further reduced to 51.7 μm. To clearly compare the effects of a pulsed current on the microstructure and mechanical response of the ultra-thin strip, ultra-thin strips with nearly the same thickness reduction were analyzed. It was found that pulsed current can reduce the degree of work-hardening of the rolled samples by promoting dislocation detachment, reducing the density of stacking faults, inhibiting martensitic phase transformation, and shortening the total length of grain boundaries. As a result, the ductility of ultra-thin strips can be effectively restored to approximately 16.3% while maintaining a high tensile strength of 1 118 MPa. Therefore, pulsed current-assisted rolling deformation shows great potential for the formation of ultra-thin strips with a combination of high strength and ductility.

Keywords: pulsed current-assisted, SUS304 ultra-thin strip, rolling reduction rate, work-hardening, mechanical properties

1. Introduction

Ultra-thin strips (0.01 mm ~ 0.1 mm) of SUS304 stainless steel are used as raw materials for key components in the aerospace, new energy, electronic communication, and medical device industries because of their excellent properties of light weight, high strength, extreme thinness, high precision, and fatigue resistance [1-2]. Nevertheless, stainless steel has high deformation resistance and is highly susceptible to work hardening, and these properties generally hinder the rolling process at room temperature, especially for ultra-thin strips. Multiple annealing treatments are effective means of eliminating deformation-induced work-hardening to obtain ultra-thin strips [3-5]. At present, SUS304 ultra-thin strips are primarily produced using multi-roll mills with high rigidity and stability, through processes involving small reductions, multiple passes, repeated rolling and continuous online annealing after rolling [6-8]. The continuous online annealing process has many disadvantages, including being resource-consuming, time-consuming and labor-intensive, and can cause serious environmental pollution problems. Therefore, seeking an efficient and environmentally friendly method to reduce the deformation resistance of SUS304 ultra-thin strips is currently a focus of research.

It has been shown that the application of a pulsed current during the plastic deformation process of metallic materials significantly enhances their plastic deformability [9-10] and decreases their work-hardening rate [11-12], thereby improving their formability [13-14] and ultimate elongation [15-16] without annealing. A preliminary exploration of pulsed current-assisted forming of SUS304 ultra-thin strips revealed that the pulsed current led to complete recovery of the plasticity of samples subjected to small deformations while reducing the strength and increasing the elongation of samples subjected to large deformations [17]. By employing a pulsed current in tensile tests of ultra-thin strips, it was found that excessive loading inhibited the martensitic phase transformation and promoted the formation of hard and brittle intermetallic compounds via solute segregation, which led to a sharp decrease in the plasticity of ultra-thin strips [18].Moreover, it has been found that the non-thermal effect produced by a pulsed current is the key to induce the reversion and recrystallization of samples at lower temperatures compared with heated tensile tests at equivalent temperatures [19]. Overall, pulsed current excitation can significantly affect the microstructural evolution and mechanical properties of SUS304 ultra-thin strips under tensile stress.

Accordingly, pulsed current-assisted rolling of SUS304 ultra-thin strips has broad industrial application prospects. The application of a pulsed current can help overcome the rolling limit for SUS304 ultra-thin strips, enabling the provision of basic materials for extreme manufacturing. However, although a high-energy electric pulse can effectively improve the plastic deformability of rolled SUS304 ultra-thin strips, the underlying reason has remained unclear [20]. At present, the degree to which a pulsed current mitigates the work-

hardening of ultra-thin strips under rolling deformation is also still uncertain. For this purpose, the pulsed current-assisted forming of SUS304 ultra-thin strips was investigated via multi-pass rolling tests in this study, and conventional rolling tests were conducted under otherwise identical conditions for comparison. The differences in the microstructures and mechanical properties of the samples rolled under the two sets of working conditions were studied to analyze the effects of a pulsed current on the deformation and work-hardening of SUS304 ultra-thin strips during rolling.

2. Materials and experimental methods

2.1 Test materials

The raw materials for the rolling tests were SUS304 ultra-thin strips with a width of 10 mm and a thickness of 115 μm, which were subjected to solid solution treatment at 1 100 °C. Their chemical composition is shown in **Table 1**. **Figure 1** shows the microstructure and morphology of a SUS304 ultra-thin strip with an average grain size (fitted ellipsoidal main diameter) of approximately 7.67 μm, which consists of recrystallized equiaxed grains and annealed twins. As shown in **Figure 1**(c), the raw material has no obvious preferred orientation, and most of the grains are randomly oriented. The maximum texture intensity is only 2.78.

Table 1. Chemical composition of SUS 304 ultra-thin strip (wt%).

Element	C	Cr	Ni	Mo	N	Si	Mn	P	S	Fe
Content	0.06	18	8.02	0.08	0.034	0.5	1.06	0.025	0.03	Bal.

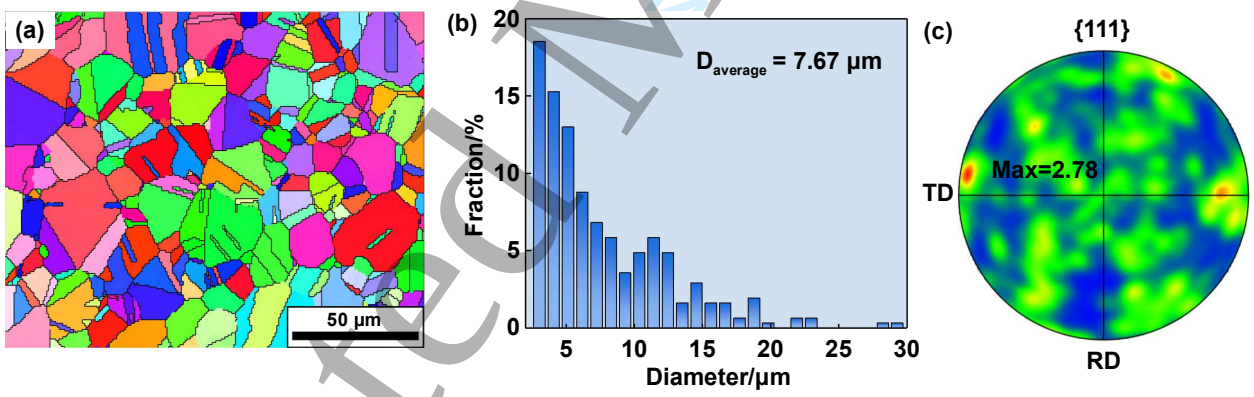

Figure 1. The microstructure of SUS 304 ultra-thin strip. (a) Inverse pole figure (IPF) diagram. (b) Grain diameter. (c) {111} pole figure, where RD and TD represent the rolling direction and transverse direction, respectively.

2.2 Pulsed current-assisted rolling tests

To construct a test platform for pulsed current-assisted ultra-thin strip rolling, a reversible twelve-roll precision cold rolling mill was modified for insulation. Based on this platform, pulsed current-assisted multi-pass rolling tests of SUS304 ultra-thin strips were conducted, following the specific test process illustrated in **Figure 2**. A YS9000DB digital programmable pulse power supply was used to apply the pulsed current to the ultra-thin strip processed through copper bars and copper clamps on both the inlet and outlet sides of the twelve-roll rolling mill, forming a closed circuit. The silicon nitride ceramic work rolls separated the mill roll

system from the ultra-thin strip, thus solving the problem of insulating the mill body (**Figure 2**(b)). High-temperature-resistant insulation tape separated the conductive copper bars, brackets, and mill body (**Figure 2**(c)). The tensiometer roll systems were treated with a high-temperature-resistant ceramic insulation coating to achieve insulation of the unwinding and winding devices (**Figure 2**(d)). Noncontact infrared temperature sensors were installed on both the inlet and outlet sides of the rolling mill to measure the temperature of the ultra-thin strip at the inlet and outlet (**Figure 2**(e)). The direct current (DC) square wave with an output current of the YS9000DB digital programmable pulse power supply is 0 ~ 600 A, the output frequency is 50 Hz ~ 2000 Hz, and the output duty cycle is 0 ~ 100% (**Figure 2**(f)).

To investigate the effects of a pulsed current on the rolling deformation of SUS304 ultra-thin strips, pulsed current-assisted rolling (ER) tests were conducted along with conventional rolling (CR) tests as a control group. The detailed rolling test parameters are shown in **Table 2**. Conventional rolling tests were conducted with the pulse power turned off, under otherwise identical rolling conditions. Both sets of tests were carried out with the same forward and backward tension (50 MPa), the same rolling speed (5 rad·s^{-1}), and the same roll gap (0.05 mm) for three round-trip passes. **Figure 3** shows a schematic diagram of the continuous rolling of ultra-thin strips.

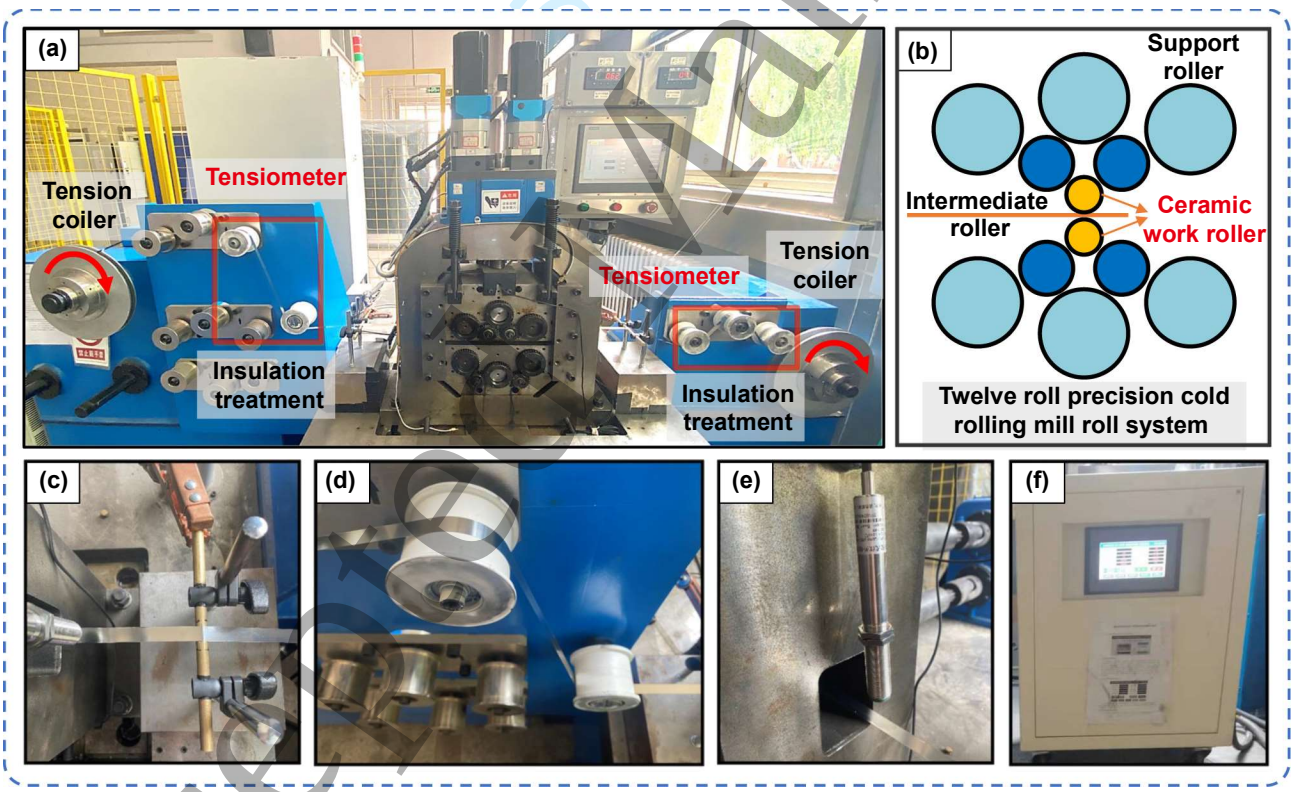

Figure 2. Layout of the rolling test platform. (a) Electric pulse assisted twelve-roll precision cold rolling mill. (b) Roll system distribution. (c) Copper clamp. (d) Insulation treatment. (e) Infrared temperature sensor. (f) Pulse power supply.

Table 2. Rolling parameters of conventional rolling and electric pulsed assisted rolling.

Sample name		Rolling passes	Thickness/μm	Cumulative strain	Pulsed current parameters	Temperature/°C
Conventional rolling	CR1	1	76.1	33.8%	0	25
	CR2	2	67.5	41.3%	0	25
	CR3	3	59.7	48.1%	0	25
Pulsed current-assisted rolling	ER1	1	67.3	41.5%	5 A, 2 000 Hz, 10%	303
	ER2	2	59.4	48.3%	5 A, 2 000 Hz, 10%	320
	ER3	3	51.7	55.0%	5 A, 2 000 Hz, 10%	335
	ER1'	1	75.6	34.2%	1 A, 1 00 Hz, 50%	87

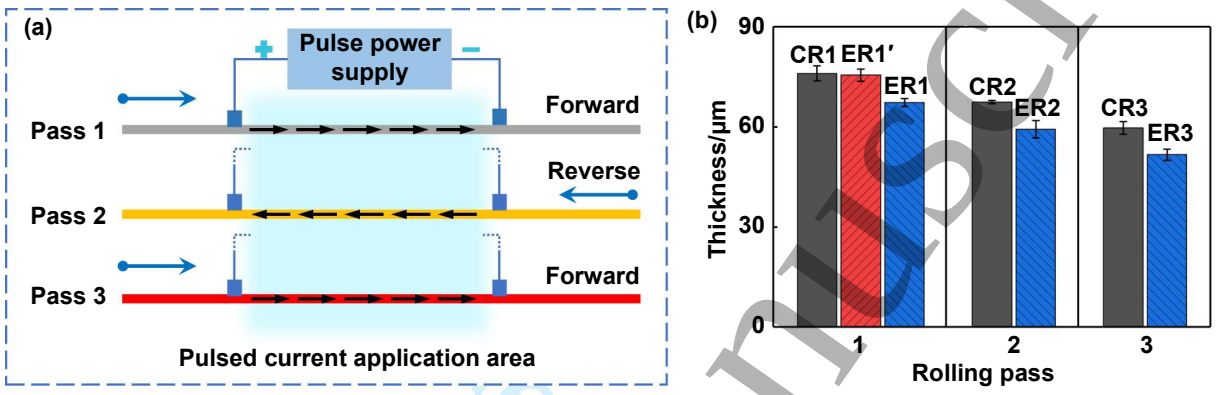

Figure 3. Multi-pass continuous rolling process for ultra-thin strips. (a) Schematic diagram of pulse current assisted rolling. (b) The thicknesses of the rolled samples after each pass.

2.3 Property testing and microstructural characterization

The thicknesses of the rolled samples were measured using a micrometer with an accuracy of 0.1 μm, and the results are shown in **Table 2**. The hardnesses of the rolled samples were determined using an HVT-1000 Vickers microhardness tester with a load of 100 g and a residence time of 10 s. The mechanical properties of the rolled samples along the rolling direction were measured using an Instron 5969 universal materials testing machine at a tensile rate of 0.3 mm·min^{-1} at room temperature. The tensile specimen dimensions were specified based on the ASTM-E8M-15 standard [21] for room temperature tensile testing, with a gauge length and width of 25 mm and 6 mm, respectively.

The volume fraction of martensite was measured using an FMP30 ferrite tester with a measurement accuracy of 0.1%. Phase characterization was performed using a DX-27mini X-ray diffractometer within the range of 30° to 100° at a scanning speed of 2°·min^{-1}. Microstructural characterization was conducted using a JEOL-IT500 scanning electron microscope (SEM) and electron backscatter diffraction (EBSD). The EBSD data were analyzed using Aztec Crystal software. The dislocation structure was observed using an FEI Talos F200X transmission electron microscope (TEM) with an acceleration voltage of 200 kV. The TEM samples were prepared by electrolytic double-spraying using a mixed solution of 10% perchloric acid and 90% alcohol. All the mechanical property tests and microscopic characterizations were repeated at least three times to ensure the accuracy and reliability of the results.

3 Results

3.1 Thickness of multi-pass rolled samples

Table 2 and **Figure 3** compare the thickness changes in the conventionally rolled samples and the samples rolled under a pulsed current. After the initial rolling, the thickness of the CR1 sample was 76.1 μm, corresponding to a thickness reduction of 33.8%. As the number of rolling passes increased, the thickness of the sample continued to decrease, and the cumulative deformation correspondingly increased. After the third rolling pass, the thickness of the CR3 sample decreased to 59.7 μm, with the cumulative thickness reduction increasing to 48.1%. For the samples rolled under a pulsed current, the thickness of the ER1 sample after one rolling pass was 67.3 μm, corresponding to a relatively large thickness reduction of 41.5%. Accordingly, the thickness of the ER1 sample was reduced by 8.8 μm compared with that of the CR1 sample. After three rolling passes, the thickness of the ER3 sample further reduced to 51.7 μm, a cumulative reduction of 55%. These results indicate that for the same number of rolling passes, the thickness of samples rolled under a pulsed current is significantly lower than that of conventionally rolled samples, thereby revealing the potential advantages of pulsed current-assisted rolling technology in improving the material deformation efficiency.

As shown in **Figure 3**, the thickness of the ER1 sample is similar to that of the CR2 sample, and the thickness of the ER2 sample is close to that of the CR3 sample. This indicates that the deformation achieved in one pass of pulsed current-assisted rolling is approximately equal to the cumulative deformation in two passes of conventional rolling. Moreover, the cumulative deformation achieved in two passes of pulsed current-assisted rolling is approximately equal to the cumulative deformation in three passes of conventional rolling. By adjusting the pulsed current parameters, the thickness of the ER1' sample is similar to that of the CR1 sample. Pulsed current-assisted rolling can effectively improve the rolling reduction rate of SUS304 ultra-thin strips, decreasing the number of rolling passes needed and enhancing the formability of the material.

3.2 Microstructure evolution

Figure 4 shows the band contrast (BC) distributions of the conventionally rolled samples and the samples rolled under a pulsed current after each pass. The BC diagram reflects the microscopic strain distribution in a sample, in which the grain boundaries and areas of strain concentration are indicated by darker colors. The average BC value represents the degree of concentration of the strain distribution in the sample, with a larger average BC value indicating a more uniform strain distribution. As shown in **Figure 4**, the average BC value of the samples gradually decreases as the cumulative deformation increases with an increasing number of rolling passes. During conventional rolling deformation, the BC value decreased from 106.3 for the CR1 sample to 75.8 for the CR3 sample, a decrease of 28.7%. During pulsed current-assisted rolling deformation, it decreased from 115.9 for the ER1 sample to 84.3 for the ER3 sample, a reduction of 27.3%. It can be seen that the proportion of strain concentration areas in the rolled samples gradually increases with an increasing number of rolling passes.

Figure 4 shows that the BC values of the samples rolled under a pulsed current are greater than those of the conventionally rolled samples after the same number of rolling passes, with the BC value of the ER1 sample being 9% greater than that of the CR1 sample. Moreover, the BC values of the samples rolled under a pulsed current are greater than those of the conventionally rolled samples with the same rolling deformation. The BC value of the ER1 sample is 36.7% greater than that of the CR2 sample of the same thickness, while that of the ER2 sample is 21.6% greater than that of the CR3 sample of the same thickness. These results show that although the thickness reduction in one pass of pulsed current-assisted rolling is already 41.5% (ER1), this modified rolling process results in fewer strain concentration areas and a more uniform strain distribution than the conventional rolling process needed to achieve the same rolling deformation (CR2).

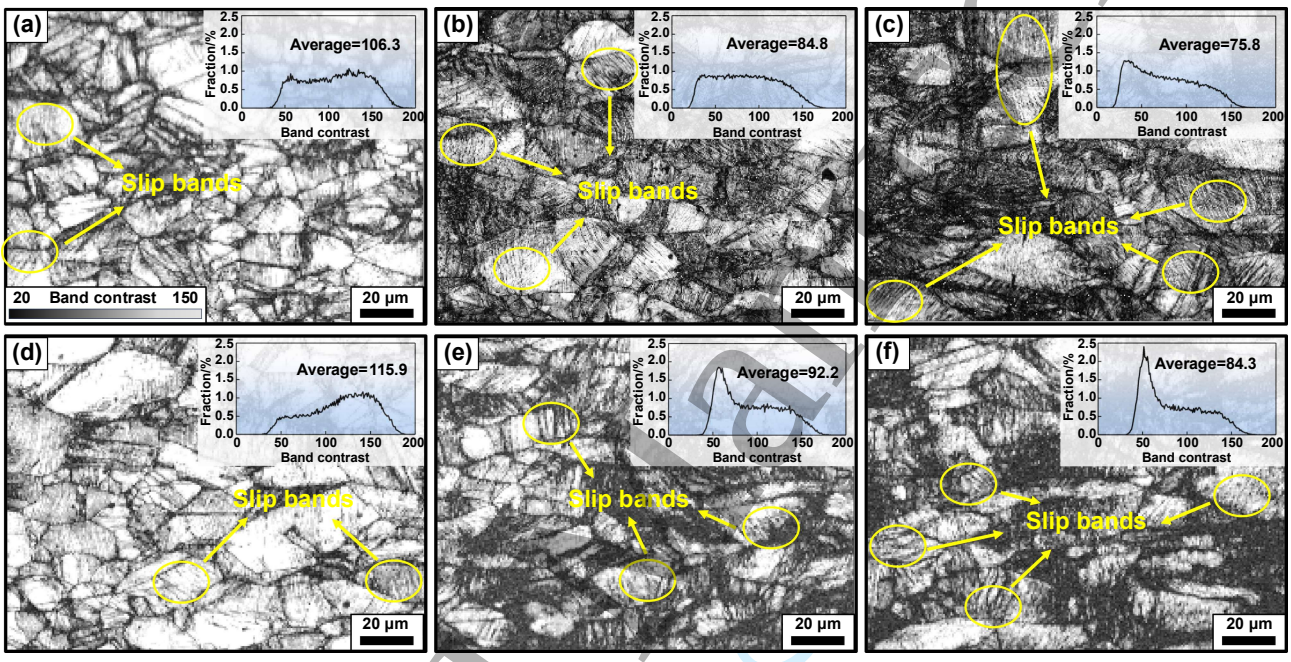

Figure 4. BC diagrams of conventionally rolled samples and samples rolled under a pulsed current. (a) CR1. (b) CR2. (c) CR3. (d) ER1. (e) ER2. (f) ER3. The top right images in the (a)-(f) show the average BC values and the BC distributions.

To analyze the effect of a pulsed current on the microstructure of SUS304 ultra-thin strips in detail, the CR1 sample, the CR2 sample, the ER1 sample, and the ER1' sample are selected for further comparative analysis, in which the thickness of the CR1 sample is the same as that of the ER1' sample, and the thickness of the ER1 sample is the same as that of the CR2 sample. **Figure 5** shows the IPF and kernel average misorientation (KAM) diagrams of the conventionally rolled samples and the samples rolled under a pulsed current. The histogram at the top right of the IPF diagram characterizes the grain size distribution. The main diameter of the fitted ellipse and the aspect ratio of the fitted ellipse along the rolling direction of the main axis were used to calculate the grain size and grain morphology. The samples were affected by the tension of the coiler and the friction shear stress of the roll in the rolling direction, which caused the long-axis average grain size and the grain aspect ratio to increase. Pulsed current can reduce dislocation accumulation and promote grain rotation. Therefore, the average grain size of the ER1' sample is 10.25 μm, while the average grain size of the CR1 sample with the same thickness reduction is 12.85 μm. With the increase in the

cumulative deformation, severe plastic deformation leads to grain fragmentation in the CR2 sample, resulting in an average grain size of only 8.98 μm. The interaction between dislocation accumulation and deformation twins generated by severe plastic deformation can lead to severe grain fragmentation and uneven grain sizes [22-23].

The KAM diagram can reflect the distributions of dislocation density and local strain in the microstructure of a sample [24]. The strain gradient model [25-26] was used to calculate the geometrically necessary dislocation (GND) density of each sample, and it was found that the distribution and change trend of the GND density were consistent with those of the KAM. The higher the KAM value is in a sample, the greater the dislocation density [27]. As shown in **Figure 5**(e)-(h), the GND densities of CR1, CR2, ER1, and ER1' are $8.31 \times 10^{14}\ m^{-2}$, $16.42 \times 10^{14}\ m^{-2}$, $9.64 \times 10^{14}\ m^{-2}$, and $5.29 \times 10^{14}\ m^{-2}$ respectively. Comparing samples with the same thickness reduction, it can be seen that the GND density of the ER1' sample is reduced by approximately 36.3% compared to that of the CR1 sample, and the GND density of the ER1 sample is reduced by approximately 41.3% compared to that of the CR2 sample. This indicates that the application of a pulsed current during rolling can reduce the dislocation density of the rolled samples.

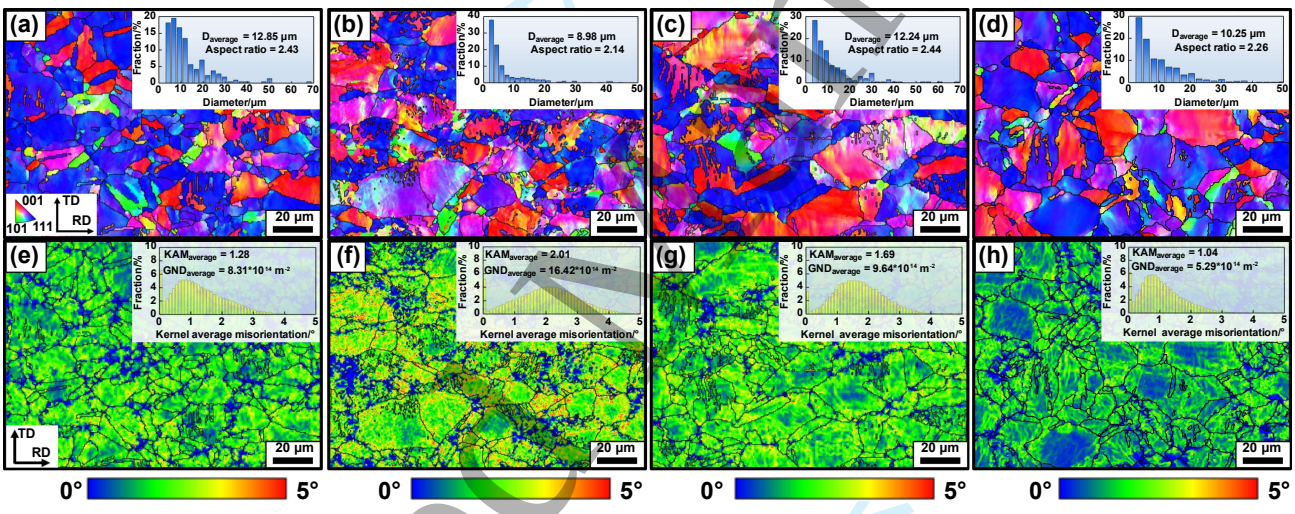

Figure 5. IPF and KAM diagrams of conventionally rolled samples and samples rolled under a pulsed current. (a) and (e) CR1. (b) and (f) CR2. (c) and (g) ER1. (d) and (h) ER1'. The top right images in (a)-(d) show the average grain size and the aspect ratio of the grains. The top right images in (e)-(h) show the average KAM and the GND density.

Figure 6 shows the grain boundary distributions and misorientation angle distributions of the conventionally rolled samples and the samples rolled under a pulsed current. The proportion of low angle grain boundaries (LAGBs) in each sample is significantly greater than that of high angle grain boundaries (HAGBs), and the average misorientation angle is less than 15°, which indicates that LAGBs are the dominant grain characteristics in all rolled samples. The formation of LAGBs is related to the dislocation walls formed by dislocation proliferation and entanglement caused by plastic deformation [28-29]. A comparison of **Figure 6**(a)-(d) shows that after the same rolling deformation, the proportion of LAGBs in the CR1 sample (69.7%) is obviously greater than that in the ER1' sample (62.8%). Similarly, the proportion of LAGBs in the CR2 sample is 78.2%, which is significantly greater than that in the ER1 sample (an increase of 7.5%). By

comparing **Figure 6**(c) and (d), it can be seen that the proportion of LAGBs in the ER1 sample is greater than that in the ER1' sample for the same number of rolling passes. This indicates that different pulsed current parameters have a significant impact on the LAGBs within the samples.

Figure 6(e) shows a comparison of the lengths of LAGBs, HAGBs, twin boundaries (TBs), and the total grain boundary length in each sample. According to the variation in the total grain boundary length, the total grain boundary length in the CR2 sample is significantly greater than that in the other samples. The lengths of HAGBs and TBs are similar in each sample. Therefore, the increase in the total grain boundary length in the CR2 sample is mainly due to an increase in the length of LAGBs. As shown in **Figure 6**(e), the length of LAGBs in the ER1 sample is significantly lower than that in the CR2 sample, which indicates that the application of a pulsed current during rolling can markedly reduce the length of LAGBs in a sample under the same rolling deformation. The length of TBs in the ER1' sample is clearly greater than that in the CR1 sample, showing that the pulsed current promotes the formation of deformation twins.

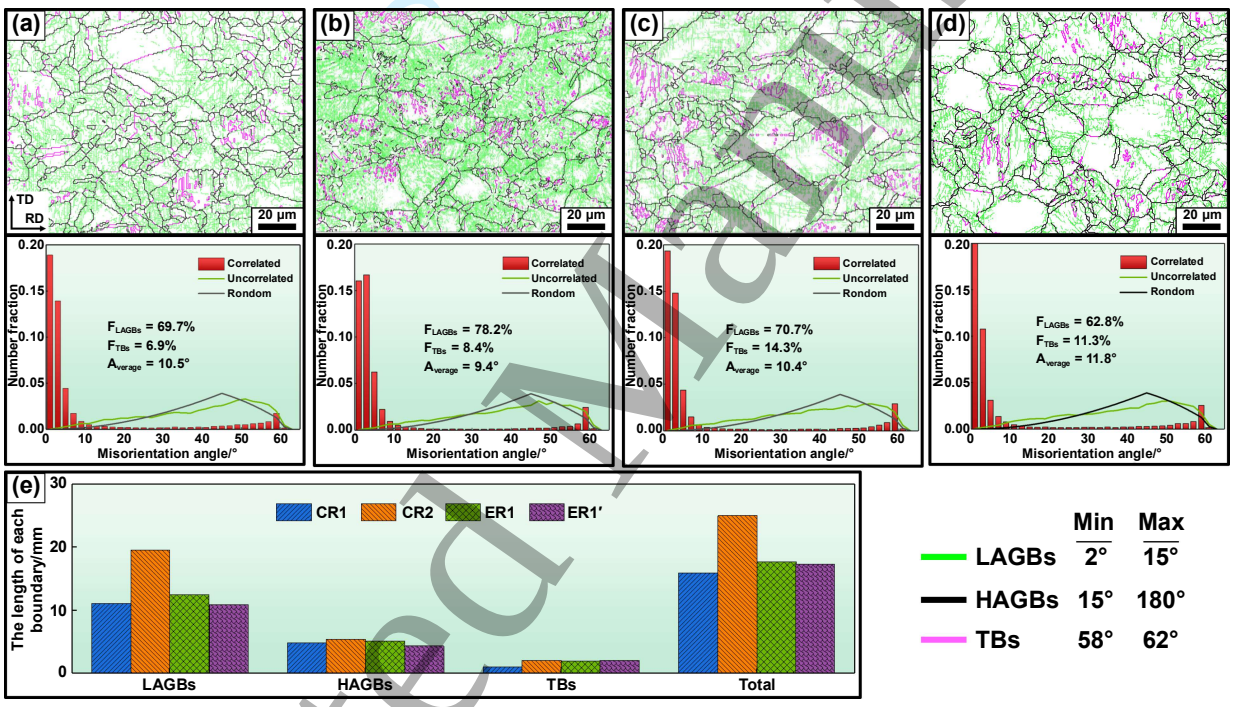

Figure 6. Grain boundary diagrams and misorientation angle distribution diagrams of conventionally rolled samples and samples rolled under a pulsed current. (a) CR1. (b) CR2. (c) ER1. (d) ER1'. (e) The lengths of LAGBs, HAGBs, TBs, and the total grain boundary length in each sample, where the LAGBs are shown as green lines, the HAGBs are shown as black lines, and TBs are shown as purple lines. In addition, 'correlated' represents adjacent grain orientation error, 'uncorrelated' represents non-adjacent grain orientation error, and 'random' represents random grain orientation error.

Figure 7 shows the orientation distribution function (ODF) diagrams of the conventionally rolled samples and the samples rolled under a pulsed current, displaying the main texture evolution of each sample. **Table 3** summarizes the common texture types of face-centered cubic (FCC) metals. The clustering of the polar density distributions is clear, indicating that obvious textures have formed in the rolled samples. As shown in **Figure 7**(a), Goss texture, Brass texture, S texture, and Copper texture with significant texture intensities have formed in the CR1 sample. On the α-orientation line, there is a significant texture aggregation

area between the Goss texture and the Brass texture. **Figure 7**(b) shows that the types of textures formed in the CR2 sample are the same as those in the CR1 sample, and their texture intensities are significantly higher. The Goss texture intensity is increased from 6.11 to 7.64, the Brass texture intensity is increased from 11.35 to 15.44, the S texture intensity is increased from 3.15 to 6.21, and the Copper texture intensity is increased from 3.64 to 7.24.

A comparison of **Figure 7**(a)-(d) shows that the texture types formed in the samples rolled under a pulsed current are the same as those in the conventionally rolled samples. Under the same rolling deformation, the texture intensity in the sample rolled under a pulsed current is lower than that of the conventionally rolled sample. Compared to those of the CR1 sample, the Goss texture intensity of the ER1' sample is 3.72, the Brass texture intensity is 8.86, the S texture intensity is 2.26, and the Copper texture is barely evident at an intensity of only 1.53. Similarly, compared to those of the CR2 sample, the Goss texture intensity of the ER1 sample is 4.48, the Brass texture intensity is 12.95, the S texture intensity is 5.53, and the Copper texture intensity is only 2.01. Thus, it can be seen that the application of a pulsed current during rolling affects the texture transitions as well as the degrees of texture aggregation in the rolled samples.

Table 3. Common types of textures in FCC metals.

Texture type	Goss	Brass	A	Rotated Goss	Copper	S
Miller index	{011} <100>	{011} <211>	{011} <111>	{011} <011>	{112} <111>	{123} <634>

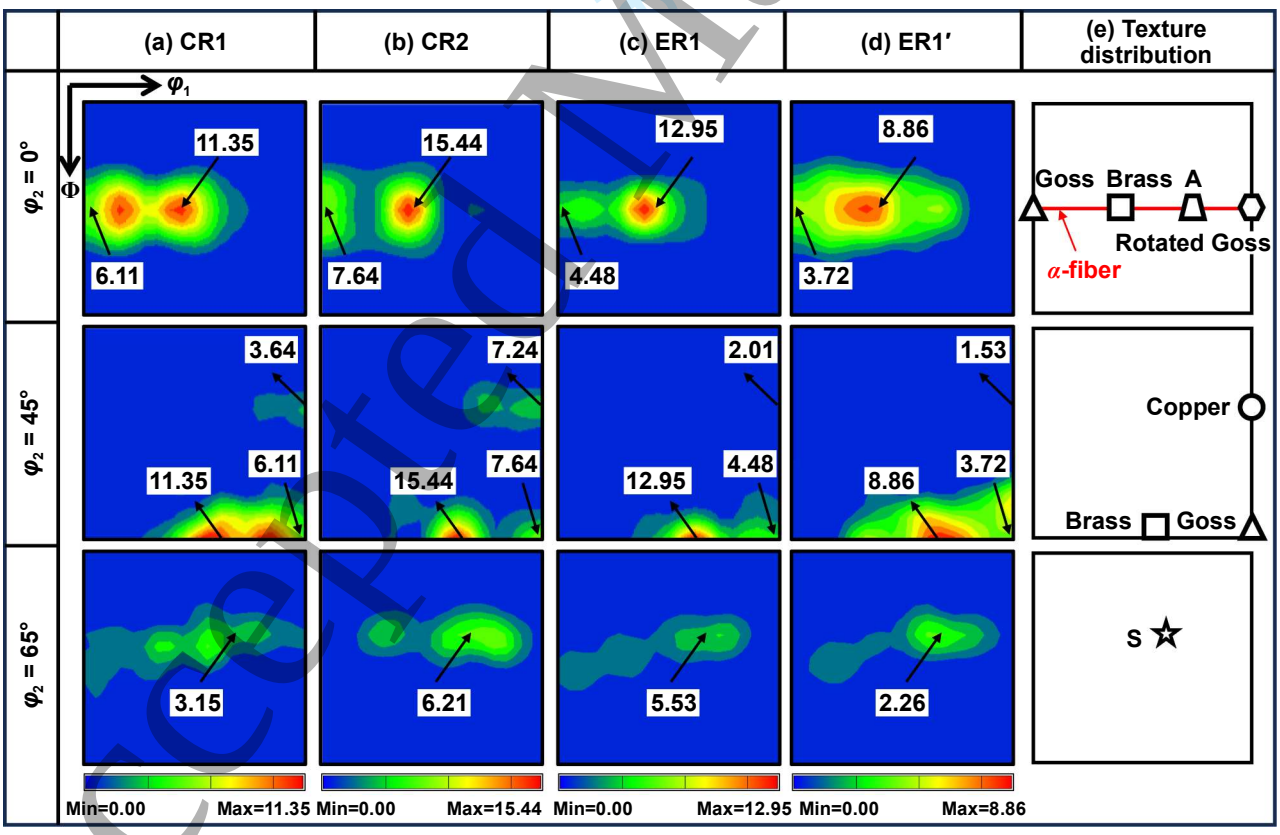

Figure 7. ODF diagrams of conventionally rolled samples and samples rolled under a pulsed current. (a) CR1. (b) CR2. (c) ER1. (d) ER1'. (e) Texture distribution.

To analyze the influence of a pulsed current on the texture evolution of the rolled samples more intuitively, **Figure 8** shows the intensities of the polar densities of each rolled sample on the α- and β-orientation lines. The Brass orientation is the intersection of the α-orientation line and the β-orientation line. When FCC metals are subjected to rolling deformation, this causes most grains to turn in the vicinity of the α- and β-orientation lines [30]. As shown in **Figure 8**, relatively complete α- and β-orientation lines formed in each sample. The β-orientation lines gradually strengthen with increasing deformation, and the grains are continuously shifted toward the Copper orientation, S orientation, and Brass orientation (**Figure 8**(b)). The Goss orientation is a sub-stable orientation, and gradually transforms into the higher-stability Brass orientation during plastic deformation. The transition from the Goss orientation to the Brass orientation can be clearly observed in **Figure 7**.

As shown in **Figure 7**, the texture intensities in the samples rolled under a pulsed current are all lower than those in the conventionally rolled samples with the same thickness. Compared with those in the CR1 sample, the Goss texture intensity in the ER1' sample is decreased by 39.1%, the Brass texture intensity is decreased by 21.9%, the Copper texture intensity is decreased by 60.0%, and the S texture intensity is decreased by 28.3%. Similarly, compared with those in the CR2 sample, the Goss texture intensity in the ER1 sample is decreased by 41.4%, the Brass texture intensity is decreased by 16.1%, the Copper texture intensity is decreased by 72.2%, and the S texture intensity is decreased by 11.0%. Among them, the decreases in the intensities of the Goss texture and Copper texture are the most significant. This is due to the formation of deformation twins within the samples rolled under a pulsed current (**Figure 6**), as the emergence of deformation twins causes the grains to rotate from the Copper orientation to the Brass orientation [31]. As shown in **Figure 4**, many slip shear bands formed during the rolling of SUS304 ultra-thin strips, and these slip shear bands drove the Goss-oriented grains to turn toward the Brass orientation. It can be seen that the application of a pulsed current during rolling promotes the emergence of deformation twins and shear band deformation in the sample, which helps to weaken the textures formed due to rolling deformation, thereby reducing the texture intensities, improving the isotropy of the sample, and enhancing its plastic deformability.

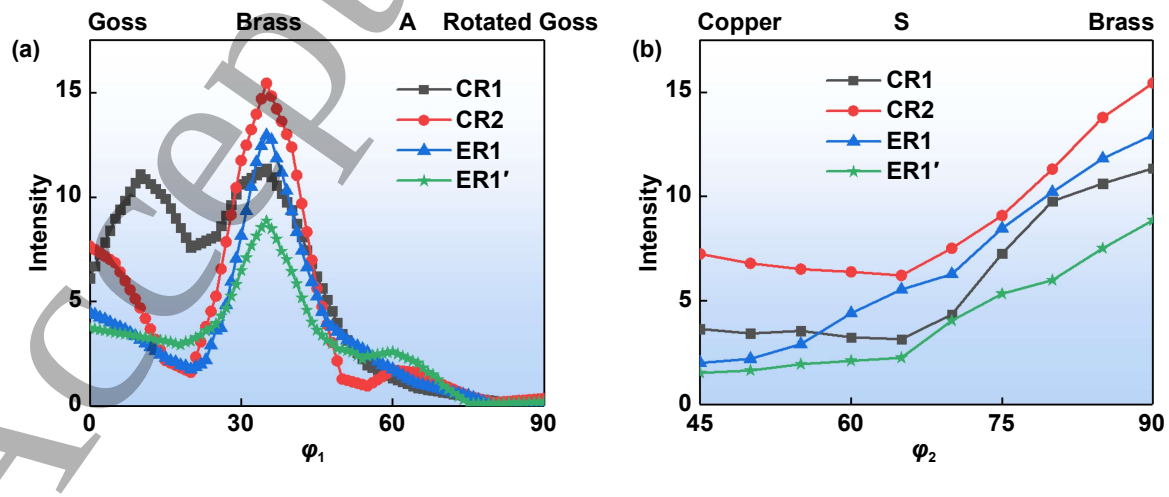

Figure 8. Comparison of polar density strength between conventionally rolled samples and samples rolled under a pulsed current. (a) α-orientation line. (b) β-orientation line.

3.3 Phase analysis

Figure 9 shows the XRD results and the volume fractions of martensite in conventionally rolled samples and samples rolled under a pulsed current after each pass. As shown in **Figure 9**(a), the intensity of the austenite diffraction peak in conventionally rolled samples gradually decreases with an increasing number of rolling passes, while the intensity of the martensite diffraction peak gradually increases. By comparing with **Figure 9**(b), it can be seen that the volume fraction of martensite in conventionally rolled samples continuously increases with increasing cumulative deformation. Compared with that in the CR1 sample, the volume fraction of martensite in the CR3 sample is increased by 4.32%.

As shown in **Figure 9**(a), the application of a pulsed current during rolling has a great impact on the diffraction peak intensity of each phase. For the same number of rolling passes, the intensity of the austenite diffraction peak in the sample rolled under a pulsed current is obviously greater than that in the conventionally rolled sample, while the intensity of the martensite diffraction peak is markedly less than that in the conventionally rolled sample. As shown in **Figure 9**(b), the volume fraction of martensite in the ER1 sample is 3.37% less than that in the CR1 sample, and the volume fraction of martensite in the ER3 sample is 6.02% less than that in the CR3 sample. Moreover, for the same rolling deformation, the volume fraction of martensite in the sample rolled under a pulsed current is markedly lower than that in the conventionally rolled sample. Specifically, the volume fraction of martensite in the ER1 sample is reduced by 5.13% compared to that in the CR2 sample of the same thickness, while the volume fraction of martensite in the ER2 sample is reduced by 6.97% compared to that in the CR3 sample of the same thickness. It can be seen that pulsed current-assisted rolling can significantly inhibit the transformation of austenite into martensite in the rolled samples.

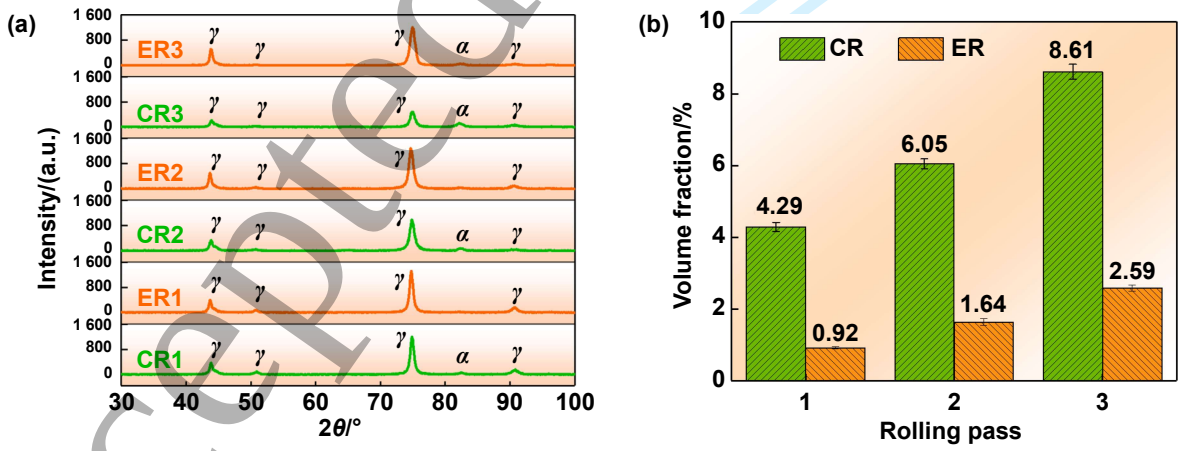

Figure 9. Comparison of phases between conventionally rolled samples and samples rolled under a pulsed current. (a) XRD pattern. (b) Volume fraction of martensite.

3.4 Mechanical properties

Figure 10 shows a comparison of the tensile properties between conventionally rolled samples and

samples rolled under a pulsed current. As shown in **Figure 10**(a), there are significant differences in the tensile curves of each sample, with different tensile strengths (TS) and elongations (EL). With an increase in the number of rolling passes, both the conventionally rolled samples and the samples rolled under a pulsed current exhibit an increase in tensile strength and a decrease in elongation. Specifically, the strength and elongation of the CR1 sample are 1 168 MPa and 10.5%, respectively, while the strength of the CR3 sample is increased to 1 426 MPa and its elongation is decreased to 3.1%. Similarly, the strength and elongation of the ER1 sample are 1 118 MPa and 16.3%, respectively, while the strength of the ER3 sample is increased to 1 315 MPa and its elongation is decreased to 3.3%. These results also show that the strength of the conventionally rolled samples is greater than that of the samples rolled under a pulsed current under the same number of rolling passes, and the elongation of the former is less than that of the latter, as shown in the inset figure in **Figure 10**(a).

Figure 10(b) shows a comparison of the mechanical properties of TRIP steel, 316 stainless steel, and IF steel [32-34], where the strength and elongation of the materials are inversely proportional to each other. The comparison of strength and elongation shows that the ultra-thin strip of electrically rolled SUS304 stainless steel produced in this study has good combined strength and elongation performance, which strongly supports the fact that the pulsed current-assisted rolling of ultra-thin strips provides an effective avenue for obtaining ultra-thin strips with controllable and exceptional mechanical performance.

Figure 11(a) presents a comparison of the strength and elongation of conventionally rolled samples and samples rolled under a pulsed current to reach the same rolling deformation. Compared to that of the conventionally rolled samples, the strength of the samples rolled under a pulsed current is slightly lower, while the elongation is significantly greater. In particular, the strength of the ER2 sample is lower by 17.3% than that of the CR3 sample of the same thickness, while its elongation is increased by a factor of 1.55; similarly, the strength of the ER1 sample is lower by 12.0% than that of the CR2 sample of the same thickness, while its elongation is higher by a factor of 1.91. These results indicate that the samples rolled under a pulsed current have excellent strength and favorable elongation.

Figure 11(b) shows the Vickers microhardness test results for each sample. The microhardness of the CR3 sample is higher by 45 HV than that of the CR1 sample, and that of the ER3 sample is higher by 54 HV than that of the ER1 sample. For the same number of rolling passes, the microhardness of the samples rolled under a pulsed current is clearly lower than that of the conventionally rolled samples. Specifically, the microhardness of the ER1 sample is lower by 29 HV than that of the CR1 sample, and the microhardness of the ER3 sample is lower by 20 HV than that of the CR3 sample. Moreover, the microhardness of the samples rolled under a pulsed current is markedly lower than that of the conventionally rolled samples with the same rolling deformation. The microhardness of the ER1 sample is lower by 43 HV than that of the CR2 sample of the same thickness, while the microhardness of the ER2 sample is lower by 37 HV than that of the CR3 sample of the same thickness. These results indicate that pulsed current-assisted rolling can significantly reduce the

microhardness of SUS304 ultra-thin strips.

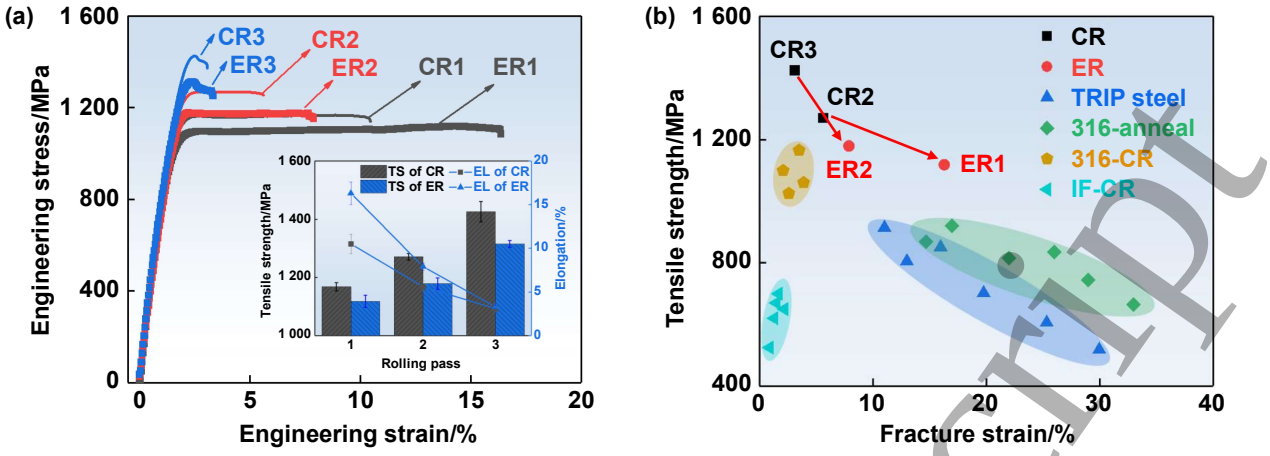

Figure 10. Comparison of mechanical properties. (a) Engineering stress-strain curves of conventionally rolled samples and samples rolled under a pulsed current. (b) Comparison of fracture strain and tensile strength in TRIP steel [32], 316 steel [33], and IF steel [34] as reported in the literature.

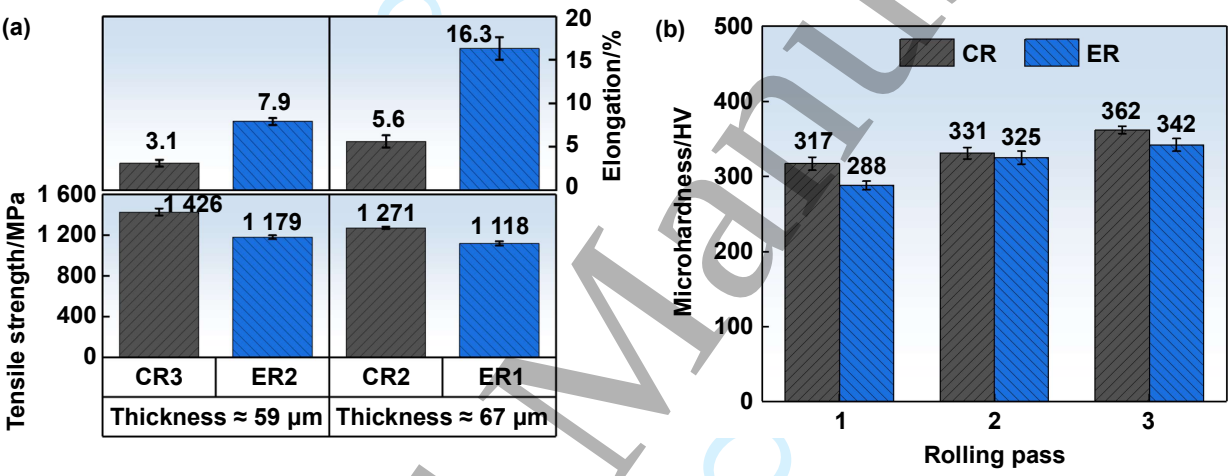

Figure 11. Comparison of mechanical properties between conventionally rolled samples and samples rolled under a pulsed current to the same thickness. (a) The tensile strength and elongation of the ER and CR samples. (b) The microhardness of each rolled sample.

Figure 12 shows the tensile fracture morphologies and section shrinkage rates of the conventionally rolled samples and the samples rolled under a pulsed current. The fracture morphology of each sample contains many ductile dimples, which are the main morphological features of metal ductile fracture [35]. As shown in **Figure 12**, the tensile fracture morphologies of the conventionally rolled samples also exhibit many scattered flat surfaces, which are caused by an uneven microstructure and the accumulation of dislocations. With increasing rolling deformation, the numbers of ductile dimples in the tensile fracture surfaces of both the conventionally rolled samples and the samples rolled under a pulsed current gradually decrease, and the section shrinkage rates gradually increase. The section shrinkage rate of the CR3 sample is as high as 83.6%, which indicates severe strength shrinkage. Combined with the elongation of each sample shown in **Figure 10**(a), it can be seen that the CR3 sample has the smallest elongation and the lowest plastic deformability, which indicates that stress concentrations can easily form in the material during tensile deformation, resulting in necking to fracture.

Upon comparing the fracture of the conventionally rolled samples and the samples rolled under a pulsed current to the same rolling deformation, it is found that the ductile fracture area of the ER1 sample is significantly larger than that of the CR2 sample. The section shrinkage rate of the ER1 sample is only 33.6%, which is notably lower than that of the CR2 sample. A greater section shrinkage rate means that stress concentrations can be more easily produced in the material during deformation, which leads to necking fracture and decreases the plastic deformability [36]. Judging from the section shrinkage rate of each sample, the ER1 sample possesses the greatest ductility. This finding corroborates the results for the tensile deformability of each sample shown in **Figure 10**(a), and further supports the conclusion that pulsed current-assisted rolling improves the plastic deformability of SUS304 ultra-thin strips.

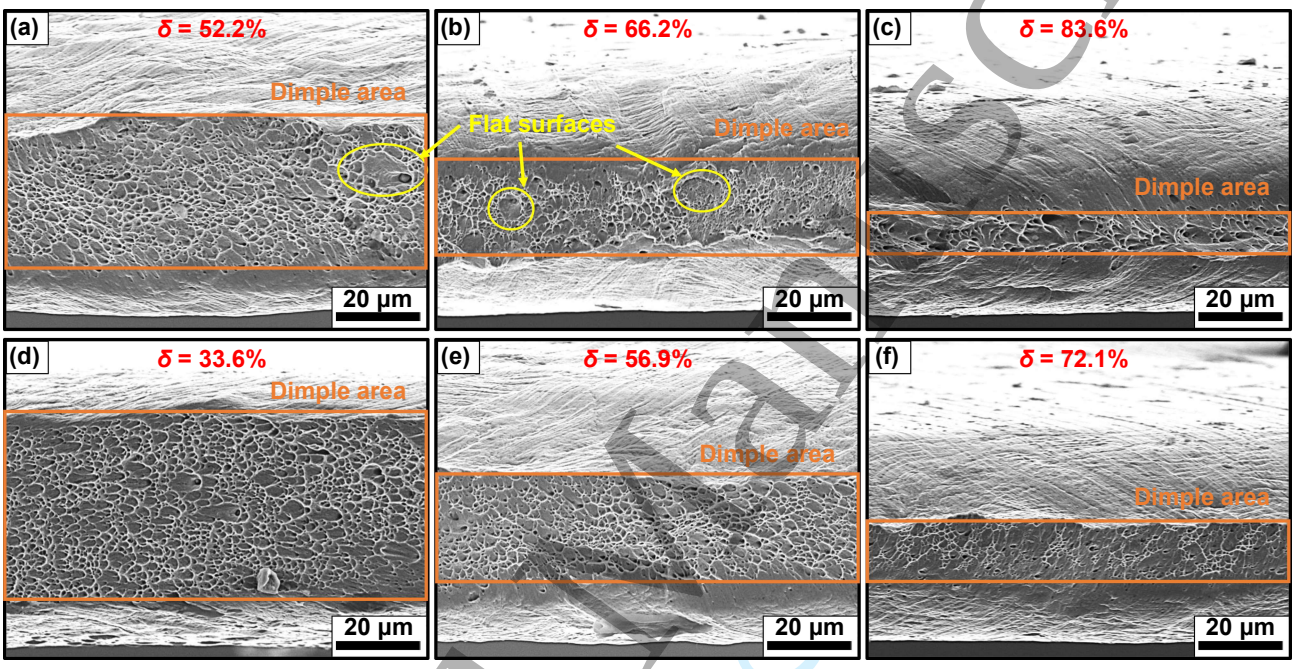

Figure 12. Tensile fracture morphologies of conventionally rolled samples and samples rolled under a pulsed current. (a) CR1. (b) CR2. (c) CR3. (d) ER1. (e) ER2. (f) ER3.

4 Discussion

The results of the present study show that pulsed current-assisted rolling can restore the ductility of 304 ultra-thin strips, consistent with the results of Lyashenko *et al.* [37], who found that pulsed current-assisted rolling helped to maintain better ductility in copper strips. Pulsed current-assisted rolling can increase the thickness reduction in each pass, reduce the degree of work-hardening and improve the plastic deformability of the processed piece.

Since work-hardening is usually considered closely related to uniform flow resistance, to quantitatively characterize the effect of pulsed current-assisted rolling on the work-hardening degree of each sample, the work-hardening index n and the strain-hardening rate $d\sigma/d\varepsilon$ were calculated using the Hollomon equation based on the true stress-strain curve:

$$\sigma = K\varepsilon^n \tag{1}$$

where K is the strength coefficient, σ is the true stress, and ε is the true strain. The work-hardening

parameters and mechanical property parameters of each sample are shown in **Table 4**. The work-hardening index is an important indicator reflecting the tensile ability of a material. A larger work-hardening index indicates that the sample is capable of producing greater uniform deformation [38]. The work-hardening index and strain-hardening rate of the ER1 sample are the largest, which indicates that the ER1 sample has better uniform plastic deformability. It is also observed that the work-hardening degree of the ER1 sample after rolling deformation is the smallest. The CR3 sample has the smallest work-hardening index, the highest tensile strength and the smallest elongation, indicating that the work-hardening degree of the CR3 sample is the largest. These results indicate that the pulsed current-assisted rolling can indeed reduce the work-hardening of the rolled samples.

Table 4. Work-hardening parameters and mechanical property parameters of conventionally rolled samples and samples rolled under a pulsed. current.

Sample name	CR1	CR2	CR3	ER1	ER2	ER3
n	~ 0.086	~ 0.046	~ 0.019	~ 0.187	~ 0.079	~ 0.054
$d\sigma/d\varepsilon$/MPa	~ 14.29	~ 11.09	~ 4.37	~ 18.83	~ 15.25	~ 8.08
TS/MPa	1 168±14	1 271±11	1 426±35	1 118±21	1 179±19	1 315±12
EL/%	10.5±1.1	5.6±0.7	3.1±0.4	16.3±1.3	7.9±0.4	3.3±0.2

The work-hardening of SUS304 ultra-thin strips is mainly caused by dislocation strengthening, phase transformation strengthening, twin strengthening, and grain refinement (grain boundary strengthening) during plastic deformation. Pulsed current-assisted rolling can reduce the degree of work-hardening of the samples, so it is speculated that the pulsed current affects the degree of work-hardening by altering the microstructures of the samples. The mechanisms by which pulsed current acts on the various microstructures of rolled samples are discussed separately below. To observe the effects of a pulsed current on the microstructures more intuitively, TEM tests were conducted on two samples with the same rolling deformation, the CR2 and ER1 samples. **Figure 13** shows the TEM images of the CR2 and ER1 samples, as well as the corresponding SAED patterns and HRTEM images.

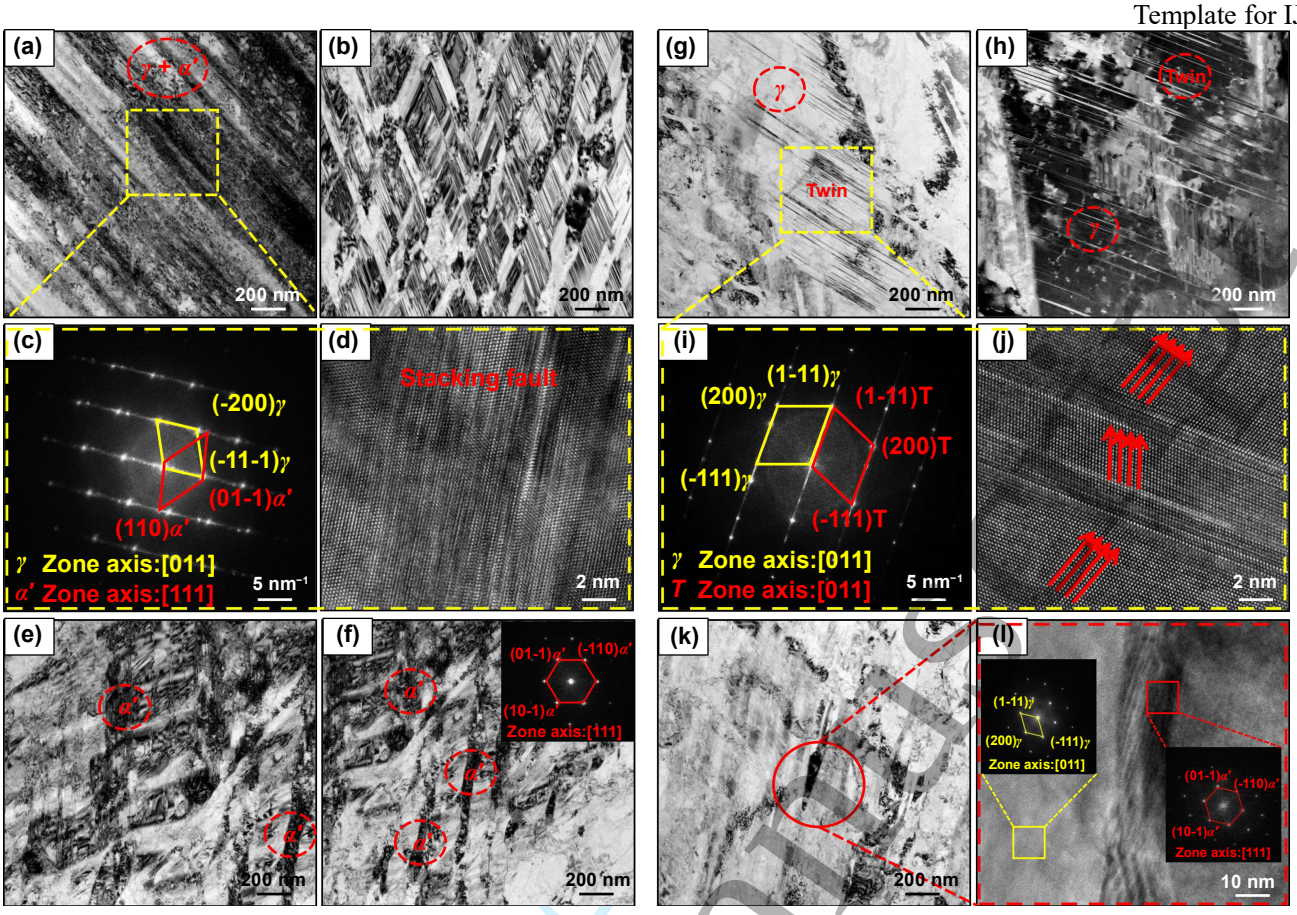

Figure 13. TEM images of conventionally rolled samples and samples rolled under a pulsed current. (a) and (b) Bright field images of the CR2 sample. (c) SAED pattern of the rectangular area marked by the yellow dotted frame in (a). (d) HRTEM image of the rectangular area marked by the yellow dotted frame in (a). (e) and (f) Martensite in the CR2 sample. (g) and (h) Bright field images of the ER1 sample. (i) SAED pattern of the rectangular area marked by the yellow dotted frame in (g). (j) HRTEM image of the rectangular area marked by the yellow dotted frame in (g). (k) Martensite in the ER1 sample. (l) HRTEM image of the elliptical area marked by the red dotted frame in (k).

Figure 13(a)-(d) show that the CR2 sample contains many stacking faults with fine intercepted units, and the martensite is observed between the stacking fault units, indicating that stacking faults and martensitic phase transformation are the main deformation mechanisms involved in the conventional rolling process of SUS304 ultra-thin strips. Under the same deformation, the stacking fault density of the ER1 sample decreases, as shown in **Figure 13**(g) and (h). And nano twins are also observed in **Figure 13**(i) and (j). The increased proportion of twins in the samples rolled under a pulsed current suggests that the source of the deformation mechanism shifts to stacking faults and twinning during the pulsed current-assisted rolling process. Based on the quantitative statistics of the LAGBs (**Figure 6**) and the GND density (**Figure 5**) in each sample, it can be concluded that the proportion of LAGBs and the GND density in the ER1 sample are lower than those in the CR2 sample. A larger proportion of LAGBs indicates that dislocation motion will be more entangled and hindered [39]. Under the same deformation, the decrease in the proportion of LAGBs and the dislocation density in the sample rolled under a pulsed current indicates that the application of a pulsed current can reduce the density of stacking faults within the sample. Due to the effect of the pulsed current, the energy of atomic motion inside the material is increased, the driving force of dislocation motion is increased, the release of entangled dislocations is promoted, and the pinning is loosened, thereby reducing the dislocation density in

the rolled sample [40-41]. Thus, the application of a pulsed current during rolling reduces the degree of work-hardening of the sample by reducing its dislocation density.

As the rolling deformation increases, many slip shear bands formed by the accumulation of dislocations appear in the material, as shown in **Figure 4**. Ferrira *et al*. [42] claimed that such slip shear bands are a prerequisite for deformation-induced martensitic phase transformation, with the intersections of the slip shear bands being the nucleation points for martensite. According to the SAED pattern in **Figure 13**(c), fine martensite formed within the layered area of the CR2 sample. In addition, there is lath martensite with the width of 50 nm ~ 100 nm within the grains of the CR2 sample (**Figure 13**(e) and (f)). As shown in **Figure 9**(b), the volume fraction of martensite in the ER1 sample is significantly lower than that in the CR2 sample. It is seen from **Figure 13**(f) and (k) that pulsed current-assisted rolling significantly inhibited the transformation of austenite to martensite. The observations show that the application of a pulsed current during rolling reduces the degree of work-hardening of the rolled samples by inhibiting the martensitic phase transformation.

With increasing rolling deformation, the interaction between dislocations, deformation twins, and martensitic phase transformation leads to fragmentation of the deformed grains [43]. Under the same rolling deformation, the grain crushing in the CR2 sample is more serious, with an average grain size of only 8.98 μm (**Figure 5**). On the one hand, the pulsed current promotes the separation and annihilation of dislocations, and reduces dislocation proliferation, leading to a decrease in the number of fragmented grains within the ER1 sample. On the other hand, the pulsed current facilitates the temperature rise of the sample, which contributes to grain growth. Consequently, the average grain size in the ER1 sample is 12.24 μm. Combined with the comparison of the total grain boundary length in each sample shown in **Figure 6**, it can be seen that the total grain boundary length in the CR2 sample is significantly greater than that in the ER1 sample. Together, these results show that the application of a pulsed current during rolling reduces the degree of work-hardening of the rolled samples by reducing grain fragmentation and the total grain boundary length.

Pulsed current-assisted rolling of SUS304 ultra-thin strips can reduce the work-hardening of the rolled samples by reducing the stacking fault density, inhibiting the martensitic phase transformation, and reducing the total grain boundary length. At the same time, the pulsed current can promote the formation of deformation twins in the rolled samples, but this has little strengthening effect. For the dislocation density of samples rolled under a pulsed current, pulsed current promotes sample softening at elevated temperature, enhances dislocation activity, frees dislocations from relatively weak constraints, and promotes dislocation motion [44]. Additionally, the pulsed current induces free electron drift, and the drifting electrons generate an additional thrust on dislocations, helping dislocations overcome obstacles, releasing dislocation entanglement, reducing the proliferation of dislocations, and promoting dislocation cancellation and rearrangement [45]. For the martensitic phase transformation of samples rolled under a pulsed current, pulsed current induces an increase in sample temperature, which helps to increase the stability of austenite and reduce the amount of martensitic

phase transformation [46]. Moreover, a pulsed current promotes the precipitation of solute atoms from the material, increases the stacking fault energy, expands the cross-slip of dislocations, and reduces martensitic nucleation [18].

In summary, pulsed current-assisted rolling helps to reduce the work-hardening of SUS304 ultra-thin strips, decrease the deformation resistance, increase the rolling reduction rate, reduce the number of rolling passes, and improve the rolling efficiency, and is expected to help overcome the present limitations on the minimum rollable thickness of ultra-thin strips. It is therefore an effective method for the production of ultra-thin strips with excellent mechanical properties that are highly efficient and environmentally friendly and save energy.

5 Conclusions

In this work, pulsed current-assisted multi-pass rolling deformation tests were carried out on SUS304 ultra-thin strips. Through comparisons with conventionally rolled samples processed under the same conditions, the resulting differences in microstructure and mechanical properties were studied, and the effect of the pulsed current on the work-hardening degree of the rolled samples was analyzed. The main conclusions are as follows:

(1) The rolling reduction rate of the conventionally rolled sample subjected to only one rolling pass was 33.8%, while the rolling reduction rate of the sample subjected to one rolling pass under a pulsed current was 41.5%. Moreover, the deformation achieved in one rolling pass under a pulsed current was approximately equivalent to the cumulative deformation in two passes of conventional rolling. This finding indicates that pulsed current-assisted rolling can significantly increase the rolling reduction rate of SUS304 ultra-thin strips, reduce the number of rolling passes, and help to improve production efficiency.

(2) The pulsed current can promote dislocation detachment, reduce the stacking fault density, decrease the martensitic nucleation caused by dislocation accumulation, increase the austenite stability, and inhibit the martensitic phase transformation. The dislocation density and the volume fraction of martensite in the ER1 sample are $9.64 \times 10^{14}\ m^{-2}$ and 0.92%, respectively, which are 41.3% and 84.8% lower than those in the CR2 sample with the same rolling deformation.

(3) Compared with conventionally rolled samples of the same thickness, samples rolled under a pulsed current have a lower stacking fault density, a smaller volume fraction of martensite, and a shorter total grain boundary length, corresponding to a lower degree of work-hardening. The ductility of the samples rolled under a pulsed current was restored to approximately 16.3%, while maintaining a high tensile strength of 1 118 MPa.

Acknowledgements

This work was supported by the fund of the National Natural Science Foundation of China (51974196), Major Program of National Natural Science Foundation of China (U22A20188), Science and Technology

Innovation Teams of Shanxi Province (202304051001025), and Central Government Guides the Special Fund Projects of Local Scientific and Technological Development（YDZX20191400002149）.

References

[1] Ren Z K, Guo X W, Fan W W, Wang T and Xiong X Y. 2020. Research progress and prospects of precision ultra-thin strip rolling theory. J. Mech. Eng. 56, 73-84.

[2] Liu X H, Zhao Q L and Yu Q B. 2018. New discoveries in micro rolling of metal foils. *Steel Rolling* **35**, 1-5.

[3] Shit G, Mariappan K and Ningshen S. 2023. Improvement of sensitization and intergranular corrosion of AISI type 304L stainless steel through thermo-mechanical treatment. *Corros. Sci.* **213**, 110975.

[4] Zhao M M, Wu H Y, Zhang B, Lu J N and Du L X. 2023. Effect of Cr-rich carbide precipitates on austenite stability and consequent corrosion behavior of ultrafine-grained 304 stainless steel produced by cryogenic rolling and annealing treatment. *Mater. Charact.* **195**, 112553.

[5] Liu X H, Song M, Sun X K, Zhao Q L and Yu Q B. 2017. Advances in research and application of foil rolling. *J. Mech. Eng.* **53**, 1-9.

[6] Qian W J. 1986. 30-High rolling mill for ultra-thin strip. *Iron Steel* **21**, 53-55.

[7] Xiao Y L. 1993. Stainless steel foil production technology of Nippon Steel. *Spec. Steel* **14**, 28-29.

[8] Zhu Y Z, Zhang Y F, Wang S Z and Wang P. 2014. Rolling of stainless steel foil. *In Proc. 2014 National Steel deep Processing Seminar.* 316-322. (The Chinese Society for Metals, Tianjin, China).

[9] Salandro W A, Bunget C J and Mears L. 2011. Several factors affecting the electroplastic effect during an electrically-assisted forming process. *J. Manuf. Sci. Eng.* **133**, 064503.

[10] Zhao Z Y, Wang G F, Hou H L, Zhang Y L and Wang Y Q. 2018. The effect of pulsed current on the shear deformation behavior of Ti-6Al-4V alloy. *Sci. Rep.* **8**, 14748.

[11] Zimniak Z and Radkiewicz G. 2008. The electroplastic effect in the cold-drawing of copper wires for the automotive industry. *Arch. Civ. Mech. Eng.* **8**, 173-179.

[12] Wang H B, Song G L and Tang G Y. 2016. Effect of electropulsing on surface mechanical properties and microstructure of AISI 304 stainless steel during ultrasonic surface rolling process. *Mater. Sci. Eng. A* **662**, 456-467.

[13] Xie H Y, Dong X H, Ai Z Q, Wang Q, Peng F, Liu K, Chen F and Wang J F. 2016. Experimental investigation on electrically assisted cylindrical deep drawing of AZ31B magnesium alloy sheet. *Int. J. Adv. Manuf. Technol.* **86**, 1063-1069.

[14] Zhao G L, Zhao B, Ding W F, Xin L J, Nian Z W, Peng J H, He N and Xu J H. 2024. Nontraditional energy-assisted mechanical machining of difficult-to-cut materials and components in aerospace community: a comparative analysis. *Int. J. Extrem. Manuf.* **6**, 022007.

[15] Salandro W A, Joshua J J, Bunget C, Mears L and Roth J T. 2015. Deformation of Metals. *In Electrically Assisted Forming* (eds Salandro W A, Jones J J, Bunget C, Mears L, Roth J T). 1-21. (Springer, Cham).

[16] Tang G Y, Zhang J, Zheng M X, Zhang J, Fang W and Li Q. 2000. Experimental study of electroplastic effect on stainless steel wire 304L. *Mater. Sci. Eng. A* **281**, 263-267.

[17] Fan W W, Ren Z K, Wei S F, Liu Q, Wang T and Wu G H. 2024. Effect of high energy electric pulse on microstructure and mechanical properties of pre-deformed SUS 304 ultra-thin strip. *Mater. Sci. Eng. A* **893**, 145364.

[18] Wang T, Wei X L, Zhang H R, Ren Z K, Gao B, Han J C and Bian L P. 2022. Plastic deformation mechanism transition with solute segregation and precipitation of 304 stainless steel foil induced by pulse current. *Mater. Sci. Eng. A* **840**, 142899.

[19] Fan W W, Liu Q, Liu W W, Wang T and Wang T X. 2023. Research on pulse current-assisted tensile deformation of SUS304 ultra-thin strips. *China Mech. Eng.* **34**, 475-480, 489.

[20] Zheng X P, Tang G Y, Song G L and Zheng Y S. 2014. Electroplastic rolling of 304 stainless steel strip. *Iron Steel* **49**, 92-96.

[21] Ren Z K, Fan W W, Hou J and Wang T. 2019. A numerical study of slip system evolution in ultra-thin stainless steel foil. *Materials* **12**, 1819.

[22] Ye K L, Luo H Y and Lv J L. 2014. Producing nanostructured 304 stainless steel by rolling at cryogenic temperature. *Mater. Manuf. Processes* **29**, 754-758.

[23] Shi Y, La P Q, Han Y J, Wei F, Sheng J and Li Z N. 2019. Rolling tuning microstructure and tensile properties of nano/micro crystalline 304 stainless steel. *Mod. Phys. Lett. B* **33**, 1950344.

[24] Ren Z K, Guo X W, Liu X, Ma X B, Jiang S Y, Bian L P, Wang T and Huang Q X. 2022. Effect of pulse current treatment on interface structure and mechanical behavior of TA1/304 clad plates. *Mater. Sci. Eng. A* **850**, 143583.

[25] Wang K H, Wang L L, Zheng K L, He Z B, Politis D J, Liu G and Yuan S J. 2020. High-efficiency forming processes for complex thin-walled titanium alloys components: state-of-the-art and perspectives. *Int. J. Extrem. Manuf.* **2**, 032001.

[26] Kubin L P and Mortensen A. 2003. Geometrically necessary dislocations and strain-gradient plasticity: a few critical issues. *Scr. Mater.* **48**, 119-125.

[27] Zhang Z C, Wang F, Yin F, Qian D S, Liu X Y and Wu M. 2023. Microstructure evolution and deformation behaviors of puls e electro-assisted deformation in M50 bearing steel. *J. Mater. Res. Technol.* **23**, 4909-4921.

[28] Zhang T, Jiang F, Huang H, Lu J, Wu Y Q, Jiang Z Y and Xu X P. 2021. Towards understanding the brittle-ductile transition in the extreme manufacturing. *Int. J. Extrem. Manuf.* **3**, 022001.

[29] Muñoz J A, Bolmaro R E, Jorge Jr A M, Zhilyaev A and Cabrera J M. 2020. Prediction of generation of high- and low-angle grain boundaries (HAGB and LAGB) during severe plastic deformation. *Metall. Mater. Trans. A* **51**, 4674-4684.

[30] De Moura A N, De Alcântara C M, Vieira E A, Rodrigues D G, Da Silva Labiapari W, Da Cunha M A, De Oliveira T R an d Orlando M T D. 2022. Microstructure and crystallographic texture of martensitic stainless steels after cold rolling and subseque nt recrystallization. *Mater. Charact.* **192**, 112190.

[31] Mao W M and Zhang X M. 1995. *Quantitative texture analysis of crystalline materials*. (Metallurgical Industry Press, Beijing), 96-118.

[32] Wang H S, Yuan G, Kang J, Cao G M, Li C G, Misra R D K and Wang G D. 2017. Microstructural evolution and mechanic al properties of dual phase steel produced by strip casting. *Mater. Sci. Eng. A* **703**, 486-495.

[33] Zhang Z X, Fu Y W, Wang T, Wang B, Xiong X Y and Wang T X. 2023. Prediction of mechanical properties of heat-treated 316l ultra-thin strip based on BP algorithm. *J. Netshape Form. Eng.* **15**, 68-77.

[34] Zhao Y, Li W J, Sun Y J and Wang M. 2022. Research on size effect of mechanical properties of IF steel during the process of preparing foil by cold rolling. *Sichuan Metall.* **44**, 6-10.

[35] Tiwari J, Prasad K, Krishnaswamy H and Amirthalingam M. 2023. Energy density to explain the ductility loss during electropla stic deformation of a dual phase steel. *Mater. Charact.* **205**, 113359.

[36] Hou J X, Zhang M, Ma S G, Liaw P K, Zhang Y and Qiao J W. 2017. Strengthening in $Al_{0.25}$CoCrFeNi high-entropy alloys b y cold rolling. *Mater. Sci. Eng. A* **707**, 593-601.

[37] Lyashenko V, Kobilskaya E and Aniskov A. 2015. Copper strip electroplastic rolling. *Metall. Min. Ind.* **2**, 294-299.

[38] Liu W H, Lu Z P, He J Y, Luan J H, Wang Z J, Liu B, Liu Y, Chen M W and Liu C T. 2016. Ductile CoCrFeNiMo_x high entropy alloys strengthened by hard intermetallic phases. *Acta Mater.* **116**, 332-342.

[39] Zhang Y L, Yang C, Zhou D S, Zhe Y, Meng L F, Zhu X K and Zhang D L. 2019. Effect of stacking fault energy on micro structural feature and back stress hardening in Cu-Al alloys subjected to surface mechanical attrition treatment. *Mater. Sci. Eng. A* **740-741**, 235-242.

[40] Li X P, Tang G Y, Kuang J, Li X H and Zhu J. 2014. Effect of current frequency on the mechanical properties, microstructure and texture evolution in AZ31 magnesium alloy strips during electroplastic rolling. *Mater. Sci. Eng. A* **612**, 406-413.

[41] Wang S P, Xiao A, Lin Y H, Cui X H and Sun X M. 2022. Effect of induced pulse current on mechanical properties and mic rostructure of rolled 5052 aluminum alloy. *Mater. Charact.* **185**, 111757.

[42] Ferreira P J and Müllner P. 1998. A thermodynamic model for the stacking-fault energy. *Acta Mater.* **46**, 4479-4484.

[43] Song R B, Xiang J Y and Hou D P. 2013. Microstructure characteristics and work-hardening mechanism of 316L austenitic stai nless steel during cold deformation. *J. Univ. Sci. Technol. Beijing* **35**, 55-60.

[44] Han C Y, Ye F, Du H Y, Liu B B, Liang Y F, Li H and Li H L. 2022. Improved ductility of Fe-6.5 wt%Si alloy under elect ropulsing tension. *Mater. Sci. Eng. A* **851**, 143639.

[45] Lee M, Yu J, Bae M H, Won J W and Lee T. 2021. Accelerated recrystallization behavior of commercially pure titanium subje cted to an alternating-current electropulse. *J. Mater. Res. Technol.* **15**, 5706-5711.

[46] Kuhfuss B, Moumi E, Clausen B, Epp B and Koehler B. 2015. Investigation of deformation induced martensitic transformation during incremental forming of 304 stainless steel wires. *Key Eng. Mater.* **651-653**, 645-650.